ACS APPLIED MATERIALS & INTERFACES

www.acsami.org

Research Article

Adhesive, Antibacterial, Conductive, Anti-UV, Self-Healing, and Tough Collagen-Based Hydrogels from a Pyrogallol-Ag Self-Catalysis System

Min Zhang, Qili Yang, Tianshuo Hu, Lele Tang, Yonghao Ni, Lihui Chen,* Hui Wu,* Liulian Huang, and Cuicui Ding*

Cite This: *ACS Appl. Mater. Interfaces* 2022, 14, 8728−8742

Read Online

ACCESS | Metrics & More | Article Recommendations | Supporting Information

ABSTRACT: Recently, versatile hydrogels with multifunctionality have been widely developed with emerging applications as wearable and implantable devices. In this work, we reported novel versatile hydrogels by self-catalyzing the gelation of an interpenetrating polymer network consisting of acrylic acid (AA) monomers and GA-modified collagen (GCOL) in situ decorated silver nanoparticles (AgNPs). The resultant hydrogel, namely AgNP@GCOL/PAA, has many desirable features, including good mechanical properties (such as 123 kPa, 916%, and 1961 J m^{-2} for the fracture stress, strain and tearing energy) that match with those of animal skin, excellent self-healing performance, favorable conductivity and strain sensitivity as a flexible biosensor, and excellent antibacterial and anti-UV properties, as well as the strong adhesiveness on skin. Moreover, AgNP@GCOL/PAA showed excellent biocompatibility via in vitro cell culture. Remarkably, AgNP@GCOL/PAA displayed superior hemostatic properties with sharply decreasing blood loss for a mouse liver incision, closely related to its strong self-adhesion which produced anchoring strength to the bleeding site and thus formed a network barrier with liver tissue. This study provides new opportunities for the facile preparation of widely used multifunctional collagen-based hydrogels based on a simple pyrogallol-Ag system.

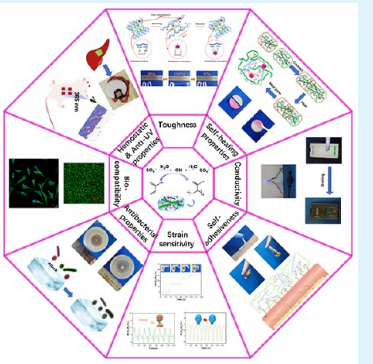

KEYWORDS: *collagen, pyrogallol, adhesive hydrogel, antibacteria, hemostasis*

INTRODUCTION

In the past decades, polymer-based hydrogels, possessing a cross-linked three-dimensional polymer network swollen by large amounts of water, have been widely exploited.[1] Of various kinds of soft matters, versatile hydrogels that were integrated with favorable adhesive, antibacterial, conductive, self-healing, and mechanical properties have attracted great interest recently because of their promising applications in wound sealing, tissue engineering, drug delivery, flexible biosensors, and bioactuators.[2−7] Nevertheless, concern has arisen that the facile fabrication of versatile hydrogels is greatly limited by the redundant synthesis of building blocks and challenges in the integration of multiple functions.

In the past few years, inspired by mussels, hydrogels based on catechol chemistry have become an important field of research, and catechol-containing molecules, typically L-3,4-dihydroxyphenylalanine (DOPA), have been widely used to fabricate adhesive hydrogels with a variety of functions. Catechol groups can form covalent and noncovalent bonds with the interface of various substrates, endowing hydrogels with strong self-adhesion ability.[8−10] Moreover, distinctive properties such as self-healing, antiswelling, and toughness properties could be introduced via the interactions between catechol groups and a series of inorganic substances (such as metal oxides) and organic substances (such as amino acids containing amine, thiol, and imidazole).[11−13] Meanwhile, with the oxidation of these inorganics or organics, the catechol groups can be converted into quinones, thereby activating persulfate to efficiently generate radicals[14] that can act as an electron-shuttle in this process.[15]

It should be noted that DOPA is derived from homopiperonylamine and phenol with prohibitive cost; moreover, there is a concern about the potential neurological effect of DOPA.[16] One promising solution to this problem is to use nature as a source of molecular libraries. Pyrogallol derivatives, which are produced by degrading plant polyphenols, are much cheaper and safer compounds compared with DOPA.[17−19] Furthermore, compared to the catechol group, pyrogallol group showed higher binding affinity for proteins or metal ions[20,21] and higher antioxidant capacity.[22] Gallic acid (3,4,5-trihydroxybenzoic acid, GA), a typical

Received: November 2, 2021
Accepted: January 30, 2022
Published: February 10, 2022

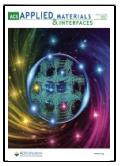

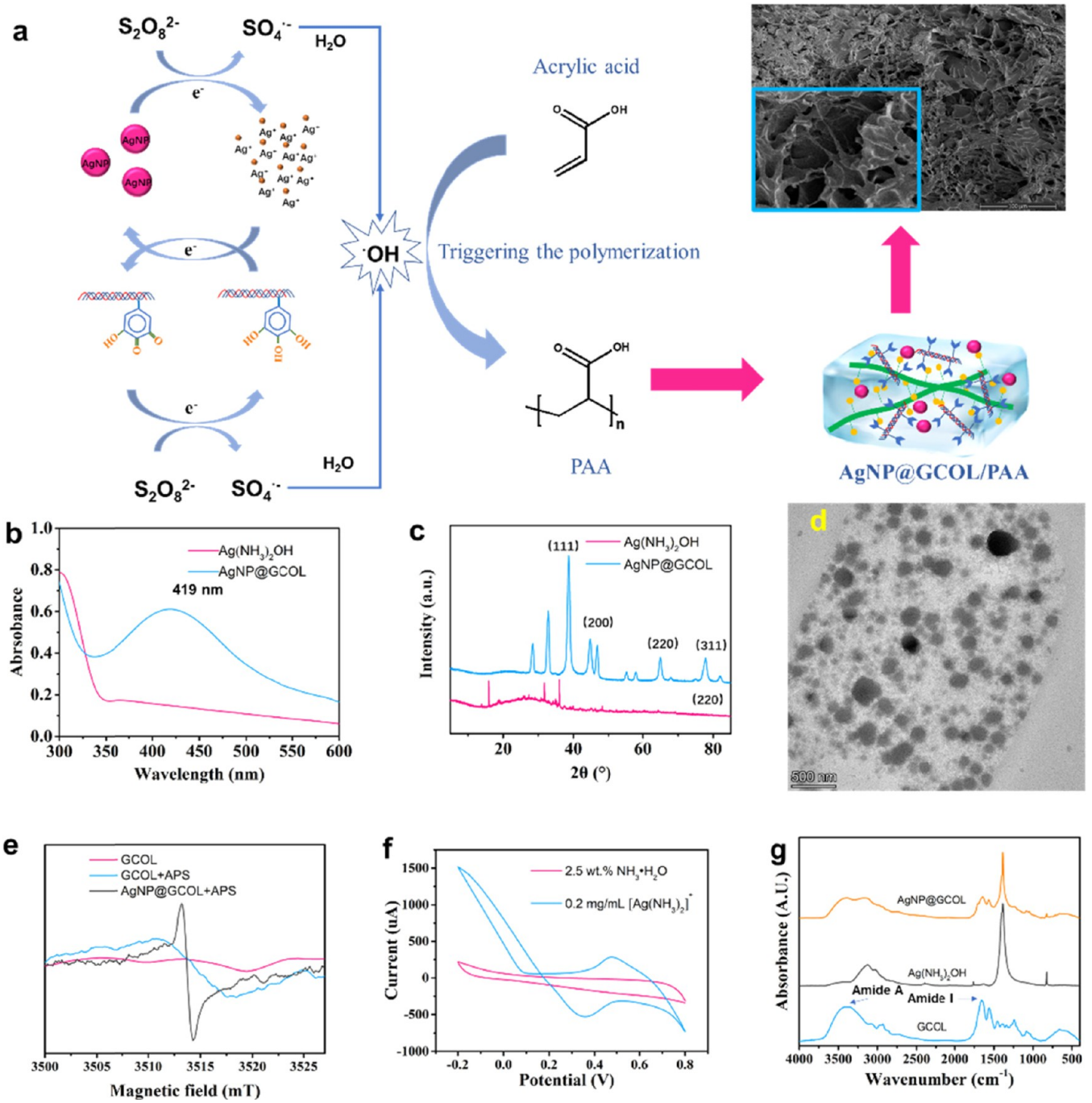

Figure 1. Design strategy for AgNP@GCOL/PAA based on the pyrogallol chemistry. (a) Schematic diagram of the self-catalysis system in AgNP@GCOL and FESEM image of the freeze-dried AgNP@GCOL/PAA. (b) UV spectra of $Ag(NH_3)_2OH$ and AgNP@GCOL. (c) XRD patterns of $Ag(NH_3)_2OH$ and AgNP@GCOL. (d) TEM image of AgNP@GCOL. (e) ESR spectra for quinone radical detection. (f) CV of the GCOL working electrode in $[Ag(NH_3)_2]OH$ and $NH_3{\cdot}H_2O$ solutions. (g) FTIR spectra of GCOL, $[Ag(NH_3)_2]OH$, and AgNP@GCOL.

pyrogallol derivative, is widely found in plants such as sumac, gallnuts, oak bark, chestnut, and so on and has been commonly used in the pharmaceutical industry.[23] Therefore, GA is a charming candidate for the construction of versatile hydrogels based on pyrogallol chemistry. Collagen is the most abundant protein in animal connective tissues and has many superior inherent characteristics such as impressive biocompatibility, low immunogenicity, and accessibility, attracting increasing attention in the biomedical field especially as wound dressing, artificial blood vessels, and skin substitutes.[24] In our previous report,[25] we designed a novel tissue glue, in which collagen was employed as the carrier of a mass of GA using ε-polylysine (EPL) as the "bridge". The basis of this study gave us inspiration to utilize the pyrogallol-containing macromolecules, namely GA-modified collagen (GCOL), as a chelating regent to form pyrogallol−metal complexes, and then to use these complexes as polymerization catalysts that self-catalyze the gelation of hydrogels in the absence of external stimuli.

Therefore, in this work, we designed a novel pyrogallol-Ag system that comprises the pyrogallol-containing macromolecules and transition metal (Ag), which can efficiently and rapidly activate ammonium persulfate (APS) to generate

https://doi.org/10.1021/acsami.1c21200
ACS Appl. Mater. Interfaces 2022, 14, 8728−8742

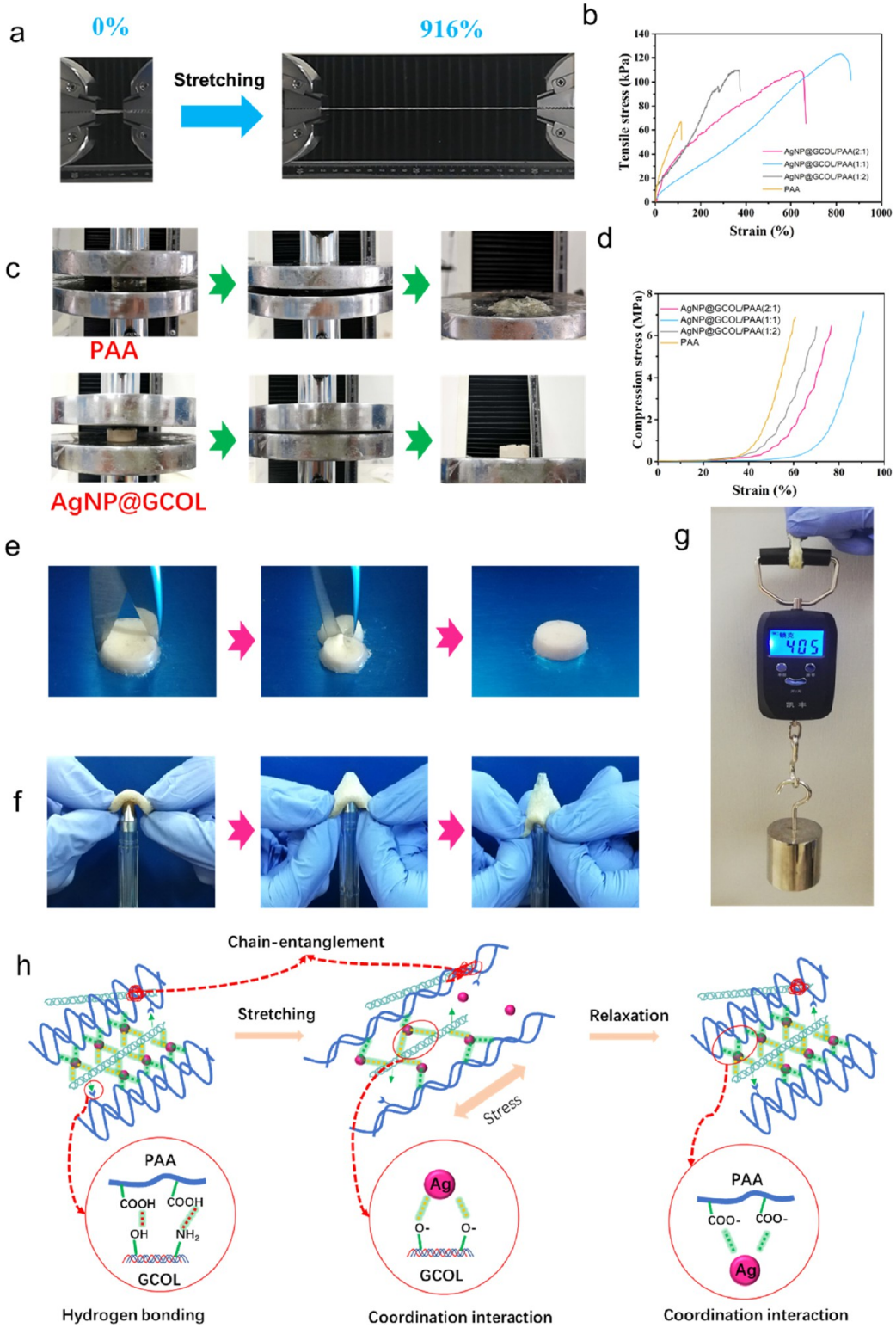

Figure 2. Mechanical properties of AgNP@GCOL/PAA. (a) Optical images of AgNP@GCOL/PAA showing high stretchability from a natural state to a stretched state. (b) Tensile stress−strain curves for AgNP@GCOL/PAA with different GCOL/AA ratios. (c) Optical images of PAA and AgNP@GCOL/PAA after undergoing a compressive deformation of 90%. (d) Compressive stress−strain curves for AgNP@GCOL/PAA with different GCOL/AA ratios. (e) Shear resistance of AgNP@GCOL/PAA. (f) Impenetrability of AgNP@GCOL/PAA. (g) Load-bearing capacity of AgNP@GCOL/PAA. (h) Mechanism on resistance to deformation of AgNP@GCOL/PAA.

radicals and initiate the radical polymerization of acrylic acid (AA) monomers, yielding a tough interpenetrating polymer network (IPN) of pyrogallol and carboxyl groups. Ingeniously, the pyrogallol-Ag system endowed the resultant hydrogels with versatile properties. In brief, the combined interactions between Ag and pyrogallol groups induced a favorable self-healing property; Ag acted as the ion transporter to make the hydrogel conductive and strain-sensitive; pyrogallol groups, Ag,

https://doi.org/10.1021/acsami.1c21200
ACS Appl. Mater. Interfaces 2022, 14, 8728−8742

and EPL gave the hydrogel an excellent antibacterial property together; an anti-UV property could also be obtained because of the existence of pyrogallol groups. More importantly, this collagen-based versatile hydrogel displayed superior hemostatic properties, closely related to its strong self-adhesion rooted in integrative interface interactions mainly from pyrogallol groups. The advantages of this design strategy are reflected in the following three aspects: (i) fast gel formation and low energy consumption, (ii) gelling conditions are not constrained to some factors, such as the depth of precursor solution in molds, UV absorption components, and the shielding effect on UV light by particles, in comparison with the widely known photoinitiated polymerization systems, and (iii) the pyrogallol-Ag self-catalysis system integrated multiple functions on the products through an easy operation. This work provides a new opportunity for the preparation of versatile collagen-based hydrogels driven by a facile pyrogallol-Ag self-catalysis strategy.

RESULTS AND DISCUSSION

Design Strategy of AgNP@GCOL/PAA. Traditionally, the process to synthesize PAA hydrogels was tedious and energy-intensive (>3 h, >50 °C) to ensure the generation of free radicals for AA monomer polymerization.[26] In addition, the pristine PAA hydrogels inherently behaved poorly in terms of mechanical properties, for instance, lack of toughness and self-healing capability.[27] For these reasons, we developed a self-catalysis system composed of GA-based macromolecules/metal ions to activate the initiators and crosslink polymer chains, so as to produce AgNP@GCOL/PAA hydrogels in a short time (within 15 min) at room temperature.

As illustrated in Figure 1a, the transition metal ion, as an oxidant, forms redox pairs with reductive pyrogallol-containing molecules. The reduced metal Ag plays a role in single-electron transfer reactions as an electron donor. Meanwhile, pyrogallol groups are good reducing agents. Therefore, together with their oxidized products (quinone), pyrogallol groups form a pyrogallol-based catalytic system as an electron donor.[28] As a consequence, AA monomer polymerization was initiated in situ to form an IPN with GCOL macromolecules under mild conditions. The morphology of the IPN observed by field-emission scanning electron microscopy (FESEM) showed a typical sponge-like porous 3D structure of the hydrogel network, which is beneficial to retain large amounts of tissue fluids and nutrients, facilitating cell penetration during the process of tissue regeneration.[29] As shown in Figure S1, the equilibrium swelling ratio of AgNP@GCOL/PAA reduced approximately by half in comparison to pristine PAA, showing a modest equilibrium swelling capacity of AgNP@GCOL/PAA which is an important feature for its use as a biomedical material. Moreover, AgNP@GCOL/PAA was not destroyed even after soaking for long times, indicating a good environmental adaptability and stability. The declined swelling ratio and improved stability could be contributed by pyrogallol groups that play a multifunctional role in forming strong noncovalent bonds and offering hydrophobicity to allow water repellence in the PAA-collagen network, which restrained the unconfined swelling behavior among the electrostatic repulsive chains of the carboxylic acid-rich PAA network.[30]

Figure 1b shows the UV−Vis curves of the aqueous suspensions of $Ag(NH_3)_2OH$ and AgNP@GCOL. Compared to $Ag(NH_3)_2OH$, AgNP@GCOL shows a characteristic peak at 419 nm owing to the surface plasmon resonance of AgNPs, confirming the generation of AgNPs.[31] Five diffraction peaks at 38.7°, 44.8°, 64.8°, 77.8°, and 81.9°, corresponding to the (111), (200), (220), (311), and (222) crystalline surfaces of silver in the format of nanoparticles (cf. standard PDF card: 65-2871) (Figure 1c), further validated the successful preparation of AgNPs. Figure 1d shows the transmission electron microscopy (TEM) image of AgNP@GCOL. It can be seen that the particle size of AgNPs ranges from ∼10 to ∼100 nm and is well dispersed in GCOL without agglomeration, which intuitively confirmed the results obtained from UV−Vis spectroscopy and X-ray diffraction (XRD) patterns. Electron spin resonance (ESR) was applied to detect the free radical generated by AgNP@GCOL. The ESR spectrum (Figure 1e) of AgNP@GCOL with APS showed a higher intensity than that of GCOL/APS, which indicated that more quinone radicals were generated in AgNP@GCOL with addition of APS.[32]

Cyclic voltammetry (CV) experiments were carried out with GCOL as the working electrode to further study the redox reaction, as shown in Figure 1f. Cyclic voltammograms of a GCOL electrode in a control electrolyte ($NH_3{\cdot}H_2O$ solution) showed no peak, while there were two redox peaks for that in the $[Ag(NH_3)_2]OH$ electrolyte, demonstrating that the phenolic hydroxyl groups of GCOL were oxidized by silver ions to quinone groups. Furthermore, Fourier transform infrared (FTIR) spectra of GCOL, $[Ag(NH_3)_2]OH$, and AgNP@GCOL were collected, and the main characteristic peaks were summarized (Figure 1g and Table S1). The peak at 3410 cm^{-1} for pyrogallol on AgNP@GCOL indicative of the characteristic absorption of O−H stretching shifted to 3390 cm^{-1} for pyrogallol on GCOL, indicating the coordination interaction between AgNPs and hydroxyl groups of pyrogallol. Also, this strong interaction affected the stretching vibration of the amide I band of pyrogallol on AgNP@GCOL, which obviously shifted to a lower wavenumber compared to that of GCOL.

Mechanical Properties of Hydrogels. We conducted tensile and compressive tests to investigate the mechanical properties of AgNP@GCOL/PAA. Figure 2a,b shows the optical images applying stretching and the stress−strain curves of the hydrogels, respectively. The fracture stress and fracture strain of AgNP@GCOL/PAA(1/1) reached 123 kPa and 916%, which were 1.3 and 2.9 times as high as those of PAA. It should be noted that the elastic modulus of AgNP@GCOL/PAA(1/1) matches that of human skin (0.1−0.5 MPa), which was vital for ideal epidermal devices[33] to accommodate the complex dynamic environment.[34] Moreover, as shown in Figure S2, AgNP@GCOL/PAA that was stretched manually to 650% could immediately return to its original length, implying an excellent self-recovery ability through energy dissipation. Figure 2c,d displays the performance of hydrogels after applying compressive deformations. Compared to PAA, AgNP@GCOL/PAA(1/1) fully recovered after removing the compression stress, implying its outstanding compressive toughness and recovery property. According to the compressive stress−strain curves, the compressive deformation exceeded 90% for AgNP@GCOL/PAA(1/1), which was obviously higher than that of PAA (60.5%), confirming its great compression recovery.

In addition, AgNP@GCOL/PAA easily suffered the force of scissors or the tip of a pen (Figure 2e,f), and a rectangular hydrogel (∼2 g) could bear weights greater than 400 g (Figure 2g). Generally, incorporating dissipation in materials can lead

https://doi.org/10.1021/acsami.1c21200
ACS Appl. Mater. Interfaces 2022, 14, 8728−8742

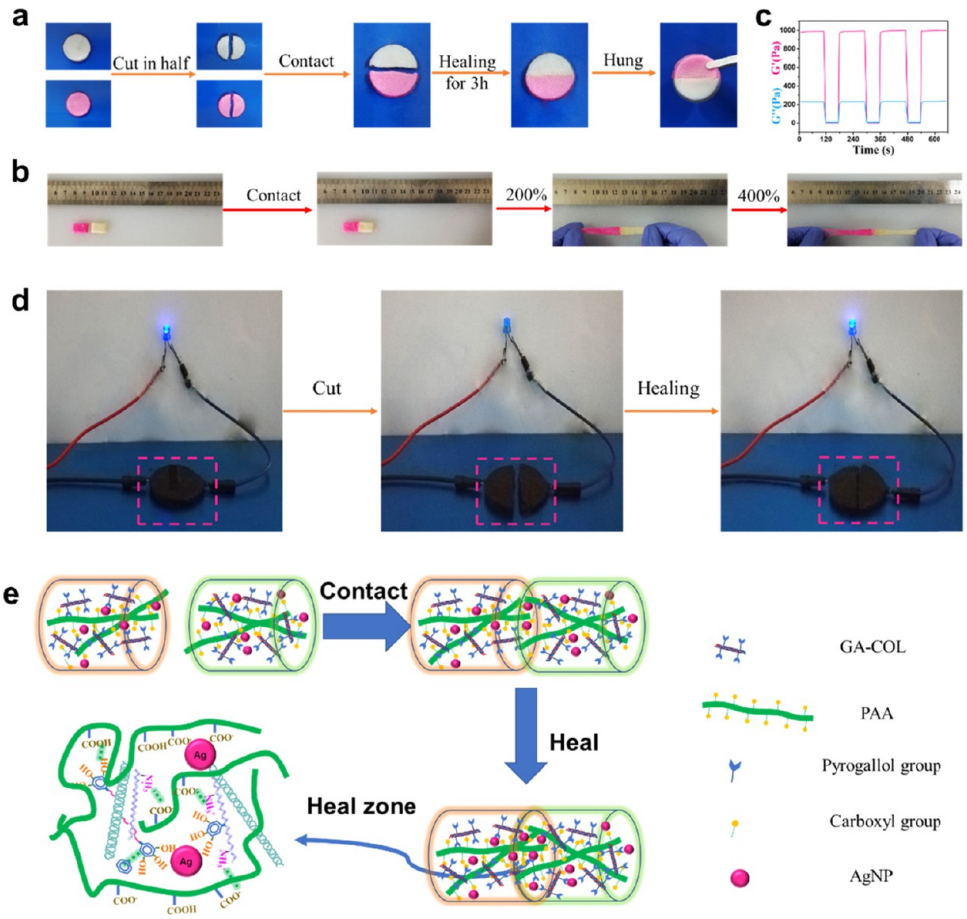

Figure 3. Self-healing property of AgNP@GCOL/PAA(1/1). (a) Photographs of the self-healed hydrogel picked up by tweezers and (b) stretched manually. (c) Self-healing property of hydrogels was studied by the step-strain test (strain = 1%/2500%/1%/2500%...). (d) Photographs of the self-healed hydrogel displaying electrical conductivity. (e) Schematic diagram illustrating the self-healing mechanism.

to high toughness.[35] As illustrated in Figure 3a, the typical tearing test, which has been widely used to measure toughness of materials such as hydrogels and elastomers, was implemented to characterize quantificationally the intrinsic toughness of the hydrogels with ensuring crack propagation through the bulk matrix. Figure S3b shows that AgNP@GCOL/PAA(1/1) possessed a significantly higher maximum tearing strength in comparison with that of the pristine PAA. Accordingly, as shown in Figure S3c, the average tearing energy for the AgNP@GCOL/PAA(1/1) was 1961 ± 98 J m^{-2}, which was 29.1 times higher than that of PAA and was quite close to that of human skin (~ 2000 J m^{-2}),[32] suggesting that the network of AgNP@GCOL/PAA has the ability to consume large amounts of mechanical energy and effectively prevent crack propagation and function failure.[35,36]

From the above results, AgNP@GCOL/PAA held desired mechanical properties that can meet the requirements of stretchable devices, which was caused by the coordination interaction in the IPN through an effectively dissipate energy dissipation path. Furthermore, in AgNP@GCOL/PAA, the dynamic entanglement effect between GCOL and PAA chains as well as the hydrogen bonds between GCOL and PAA also served as sacrificial bonds to dissipate energy during the deformation process.[30,37] Meanwhile, the irreversible covalent PAA network maintained the structural integrity by avoiding nonrecoverable damage, as shown schematically in Figure 2h.

Self-Healing Behavior and Conductivity. Self-healing ability is of great importance for hydrogels applied as wound repair dressings or implantable electronics.[38] First, AgNP@GCOL/PAA was remolded to disks, which proved its excellent deformability. Then red and white disk-shaped samples were cut into two halves, and two pieces of different colors physically in contact can recombine into a new one at ambient temperature without any stimuli (Figure 3a). Note that the self-healed rectangular sample was stretched to four times its original length without rupture (Figure 3b), suggesting an excellent self-healing property. The step-strain measurement for AgNP@GCOL/PAA was further carried out to evaluate the self-healing ability quantitatively. First, the intersection point of elastic modulus (G′) and viscous modulus(G″) as a function of strain of the hydrogel was measured (Figure S4), which was at a strain of 2479%, suggesting that the hydrogel network begins to break down at this critical point.[39] Next, the step-strain test for AgNP@GCOL/PAA was conducted with small and large strain fixed at 1 and 2500%, respectively (Figure 3c). AgNP@GCOL/PAA showed stable G′ and G″ values under small strain, and when the oscillating strain jumped to 2500%, G′ and G″ dropped precipitously, while both of them promptly returned to their original state after the strain returned back to 1%. It is worth noting that G′ and G″ of AgNP@GCOL/PAA still retain their original level after three step-strain cycles, demonstrating its superior self-healing ability.

https://doi.org/10.1021/acsami.1c21200
ACS Appl. Mater. Interfaces 2022, 14, 8728−8742

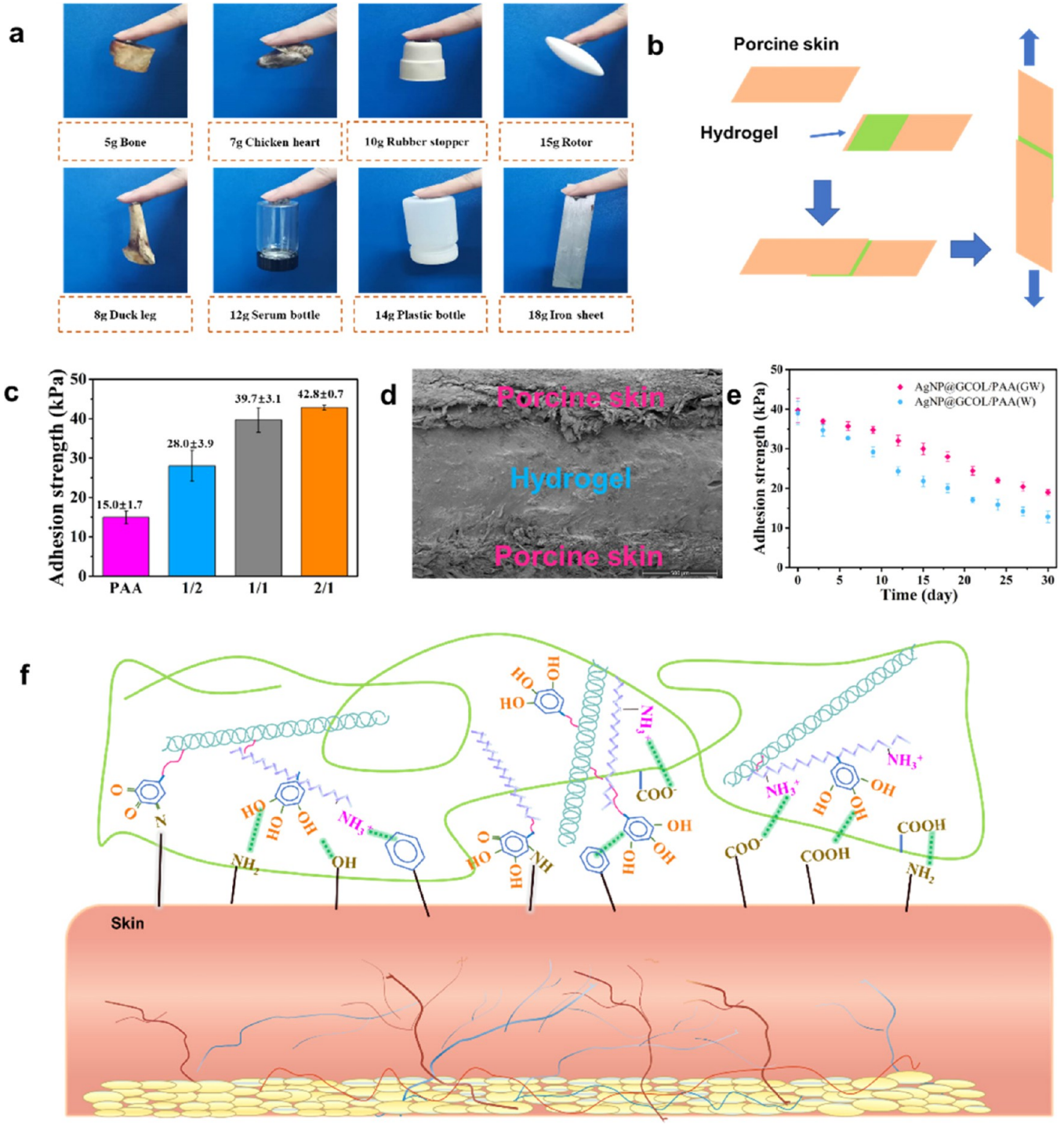

Figure 4. Adhesive properties of AgNP@GCOL/PAA. (a) Digital photos of AgNP@GCOL/PAA adhering to various material surfaces and tissues. (b) Schematic illustration of the lap-shear adhesion test. (c) Adhesion strength of various AgNP@GCOL/PAAs to porcine skin (n = 5). (d) FESEM image of cross-sectional fracture morphology of the adhered porcine skins. (e) Adhesion strength of AgNP@GCOL/PAA with increasing storage times. (f) Schematic illustrating the molecular mechanism of AgNP@GCOL/PAA adhering to tissue surfaces.

The self-healing behavior of AgNP@GCOL/PAA was further confirmed by a conductivity test (Figure 3d). First, the effect of AgNPs on the conductivity of the hydrogels was investigated using the four-probe method,[40] and the results can be referred to Table S2. Because of the dissociation of carboxyl groups, the pristine PAA hydrogel exhibited a weak conductivity, while AgNP@GCOL/PAA with an $AgNO_3$ dose of 50 mg/mL possessed a conductivity more than three times that of pristine PAA, and also higher than those of chitosan/polyacrylamide and gelatin/polyvinyl alcohol (~4 mS/cm),[41,42] which indicated that the presence of AgNPs greatly promotes the electrical conductivity. Next, AgNP@GCOL/PAA was connected to a light-emitting diode (LED) bulb with a built-in power supply. As expected, the LED bulb illuminated as soon as the conductive AgNP@GCOL/PAA formed a closed circuit. Then, AgNP@GCOL/PAA was cut from the middle and the bulb immediately went out. Note, however, that, once the freshly cut halves touched, the bulb

https://doi.org/10.1021/acsami.1c21200
ACS Appl. Mater. Interfaces 2022, 14, 8728−8742

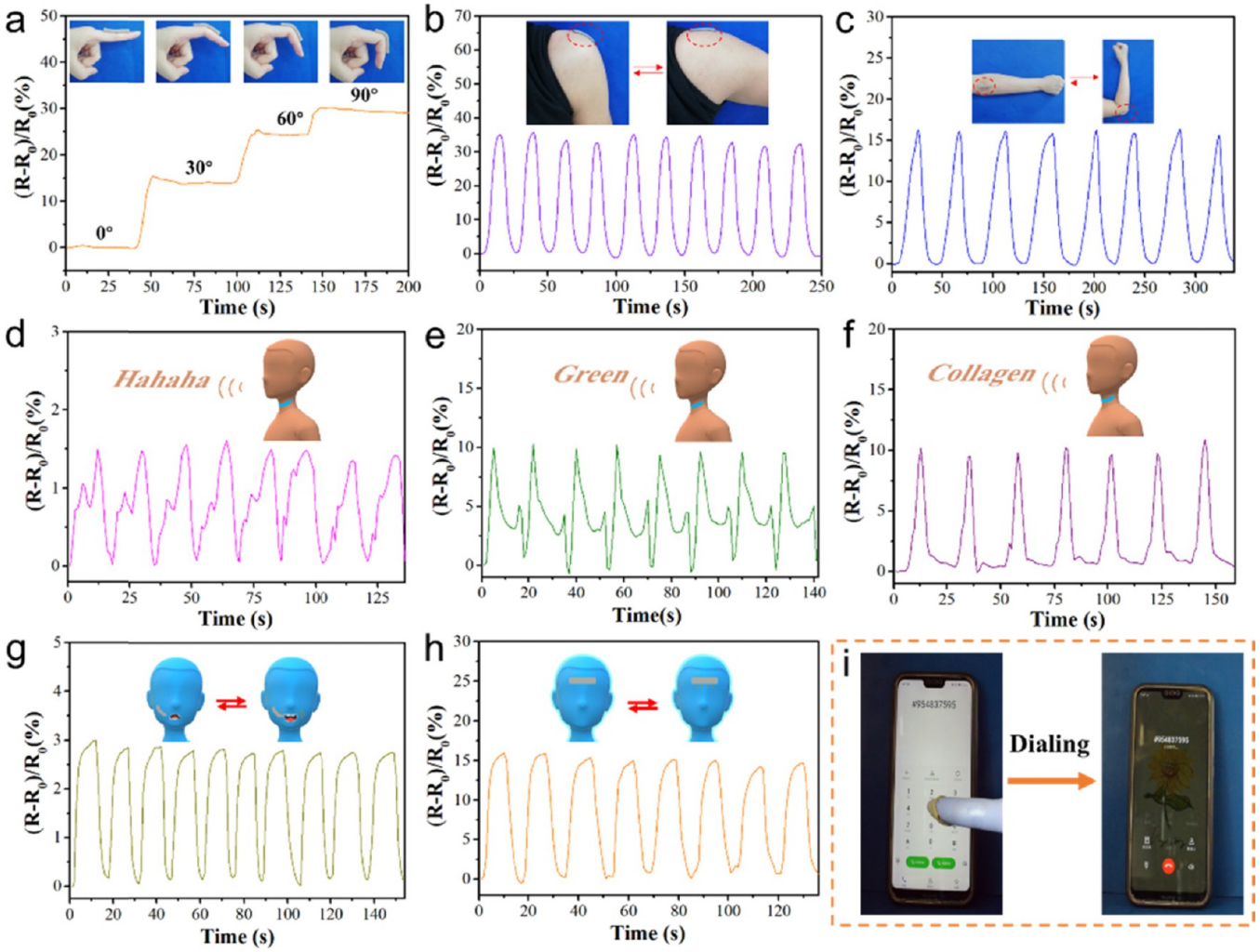

Figure 5. Performance of AgNP@GCOL/PAA as a skin sensor. The monitored relative resistance changes of the on-skin sensor attached on a human finger with different bending angles (a), on shoulder with different extending angles (b), on elbow with different bending angles (c), and on throat when pronouncing "Ha," "Green," and "Collagen" (d,e,f). Relative resistance changes from facial expression change-smile (g) and forehead wrinkles (h). (i) AgNP@GCOL/PAA was used as an electronic skin to dial a mobile phone number.

was promptly illuminated again, suggesting the fast self-healing ability of AgNP@GCOL/PAA.

Typically, self-healing performance of materials is achieved by designing reversible bonds.[43−46] As illustrated in Figure 3e, in this work, reversible hydrogen bonds and coordination bonds among GA-modified collagens, PAA chains, and Ag nanoparticles made the hydrogel of feasible self-healing capacity without any external stimuli.

Adhesion Properties of AgNP@GCOL/PAA. The lap-shear strength tests were applied to assess the self-adhesive property, and the porcine skin was used because of its similarity to human dermis. As shown in Figure 4a, the hydrogels tightly adhered to a bovine bone, a chicken heart, and various other substrate surfaces, including rubber, polytetrafluoroethylene, glass, plastic, and metal. The process of lap-shear strength measurement is illustrated in Figure 4b, and the corresponding results are shown in Figure 4c. It can be observed that the values of adhesive strength increased with the GCOL/AA ratio, owing to the increased amount of phenolic hydroxyl groups. Note that all the adhesion strengths of AgNP@GCOL/PAA were greatly larger than that of commercial porcine fibrin sealant (2.5 ± 0.8 kPa).[25] The strong adhesion of AgNP@GCOL/PAA to skin was further studied by the FESEM image from the adhered sandwich sample (Figure 4d).

In addition, the changes in the adhesive strength of AgNP@GCOL/PAA (2/1) as a function of time were assessed. For comparison, AgNP@GCOL/PAA (2/1) without glycerol was prepared as a control. As shown in Figure 4e, the adhesion strength of AgNP@GCOL/PAA (2/1) retained more than 50% of the original value at day 30, which was higher than that of the control sample (~40%). Meanwhile, as shown in Figure S5, the rate of water loss of the sample containing glycerol was less than 10% after 30 days; meanwhile nearly 50% of that for the sample without glycerol was measured. Therefore, the loss in adhesiveness is probably due to the reason: the polar groups on the surface of the hydrogel became increasingly reluctant to be exposed as moisture is lost, causing the greater loss of adhesive strength.[47]

The desired adhesion performance is closely correlated with the formation of sufficient interface interactions, which are illustrated in Figure 4f. In this IPN, strong $\pi-\pi$/cation$-\pi$ interactions formed between the benzene rings of GA and the tissue interface.[48,49] Furthermore, quinone groups produced by the oxidation of gallol groups can combine with the amino groups from the pig skin, resulting in strong interfacial

https://doi.org/10.1021/acsami.1c21200
ACS Appl. Mater. Interfaces 2022, 14, 8728−8742

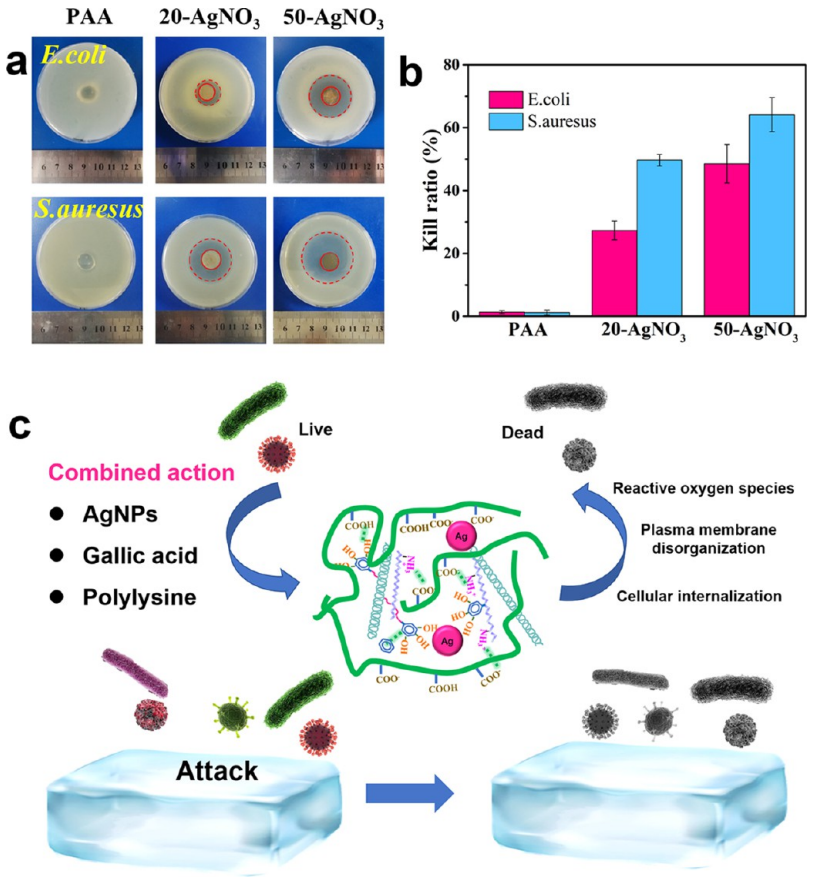

Figure 6. Antibacterial ability of AgNP@GCOL/PAA. (a) Antibacterial ring of *E. coli* and *S. aureus* for AgNP@GCOL/PAA. (b) Antibacterial ratios of AgNP@GCOL/PAA to *E. coli* and *S. aureus* (n = 5). (c) Schematic diagram illustrating the antibacterial mechanism of AgNP@GCOL/PAA.

interactions, including Michael addition and Schiff base.[50,51] Moreover, phenolic hydroxyl groups acted as hydrogen bond donors to enhance bioadhesive capability.[52] In addition, hydrogen bonding or electrostatic interaction can also occur between carboxyl groups in PAA and amino groups in tissue.[48]

Strain Sensitivity of AgNP@GCOL/PAA as a Sensor. The self-adhesive and conductive AgNP@GCOL/PAA was applied to attach onto human skin for 30 min and then strip away, without any residue and allergic reaction on the arm (Figure S6). This demonstrated that AgNP@GCOL/PAA possessed excellent skin conformability.

Considering its suitable modulus, feasible conductivity, adhesiveness, and skin conformability, AgNP@GCOL/PAA has potential to be applied in human−machine interactions as an epidermal skin sensor. We attached AgNP@GCOL/PAA onto human skins to monitor the physiological activities, including macroscale movements such as bending of fingers and arm joints and microscale motions such as vocal-cord vibration and facial expressions. As shown in Figure 5a, the hydrogel can be compliantly self-adhered onto the finger knuckle, and the relative resistance synchronously jumped to corresponding values in a stepwise manner, as the bending angle increased from 0° to 30° to 60° and to 90°. This is because the elastic deformation of the hydrogel induced a significant change in the distance between adjacent AgNPs, which gradually weakened the conductivity of the hydrogel, therefore resulting in an increase in the relative resistance variation of the hydrogel as the bending angle increases.[53] Moreover, the periodic changes of signals upon the bending and extending stimuli of the human shoulder and elbow were well detected in real time, showing a regular "wave" shape (Figure 5b,c), suggesting the high sensitivity and stability of AgNP@GCOL/PAA as a sensor. Furthermore, the hydrogel sensor was able to detect the vibration of the vocal cords with high resolution when the volunteer said "ha" "green" and "collagen" repeatedly (Figure 5d,e,f). It could be found that the monosyllabic and three-syllable words were converted into corresponding electrical signals with characteristic speech patterns.

It is a challenge for facial expression recognition through strain sensors because of the complex muscle groups, low modulus of facial skin, and low deformations of common expressions.[53] As illustrated in Figure 5g,h, regular and stable signals of relative resistance were generated when the volunteer smiled and frowned repeatedly, confirming the successful detection of subtle human activities. Note that the hydrogel could smoothly detect the microstrains (<0.3%) of writing with a pen (Figure S7), illustrating its large working range and stable working ability as a sensor. In addition, AgNP@GCOL/PAA could be used as an electronic skin to mimic the function of human skin. As shown in Figure 5i, after the hydrogel was attached to the finger, it can operate a smartphone to dial numbers smoothly, demonstrating the great potential of this hydrogel in robotic e-skin, human−computer user interfaces, and flexible electronics.

Antibacterial Activity of AgNP@GCOL/PAA. Hydrogels possess a high content of water, prone to trigger the growth and reproduction of bacteria. Hence, the antibacterial activity

https://doi.org/10.1021/acsami.1c21200
ACS Appl. Mater. Interfaces 2022, 14, 8728−8742

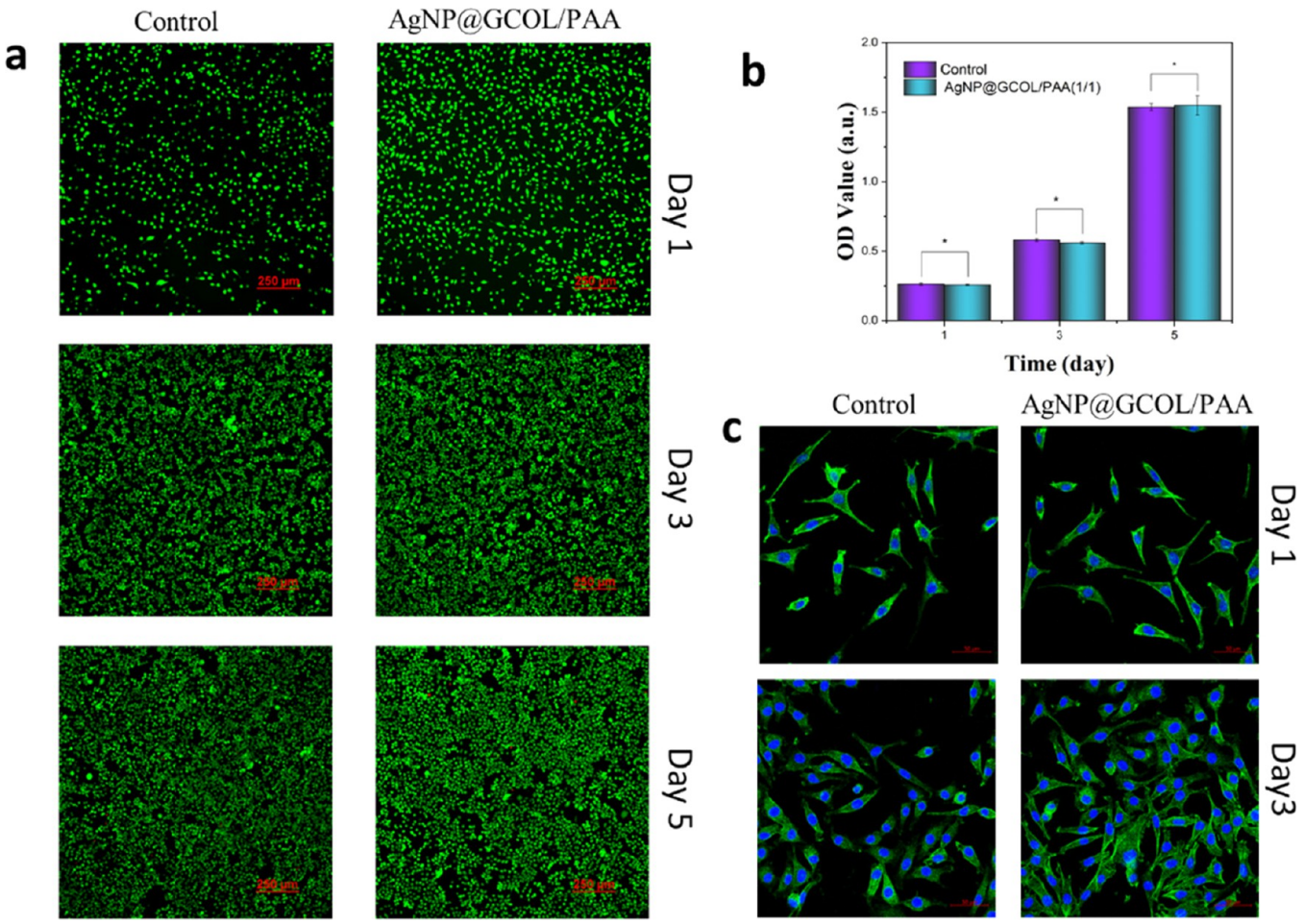

Figure 7. (a) Representative live/dead staining images of L929 fibroblast cells on days 1, 3, and 5. (b) Cell viability study using L929 fibroblast cells via CCK-8 assay on days 1, 3, and 5 (*$p < 0.05$). (c) Cytoskeleton staining of L929 fibroblast cells after 1 and 3 days of culture in vitro (DAPI, blue; phalloidin, green).

is one of the key performances for hydrogels in practical application. The antibacterial ability of AgNP@GCOL/PAA against both *Escherichia coli* and *Staphylococcus aureus* was measured. Figure 6a shows the antibacterial rings, from which we found that the two kinds of bacteria were efficiently inhibited. The diameter of antibacterial rings for *E. coli* and *S. aureus* at 20 mg/mL of $AgNO_3$ was 20 and 33 mm, while the corresponding parameter at 50 mg/mL of $AgNO_3$ increased to 33 and 40 mm, respectively, indicating an improved antibacterial ability of AgNP@GCOL/PAA upon increasing the content of AgNPs. Note that the control group (PAA) did not show any antimicrobial effect. For quantitatively studying the antibacterial activity, the bacteriostatic rate was determined after the bacterial fluid came in contact with AgNP@GCOL/PAA for 24 h at 37 °C. As shown in Figure 6b, approximately 50% of *E. coli* and 65% of *S. aureus* were killed at 50 mg/mL of $AgNO_3$, which were consistent with the results of antibacterial rings.

It is well known that AgNPs, GA, and EPL all possess bactericidal activity. Haidari et al. found that AgNPs exerted powerful antibacterial effects mainly through interaction with the bacterial membranes to cause structural damage and membrane depolarization, as well as downstream metabolism.[54] Sun et al. studied that GA can damage the bacterial membrane, causing the leakage of the contents of the bacteria, which in turn affects the growth of the bacteria and causes their death;[55] EPL is a well-known cationic biomacromolecule, which can be used for enhancing penetration through (negatively charged) cell membranes, destroying the bacterial membrane structure, thereby inhibiting the growth of *E. coli and S. aureus*.[56,57] Based on these effects, AgNP@GCOL/PAA showed strong antibacterial activity as expected (Figure 6c).

Biocompatibility and In Vitro Biodegradability of AgNP@GCOL/PAA. We evaluated the cytocompatibility of AgNP@GCOL/PAA(1/1) through the live/dead, CCK-8 assay, and cytoskeletal staining. As shown in Figure 7a, the L929 fibroblasts exhibited normal fusiform morphology. For AgNP@GCOL/PAA, the images showed predominate live cells (green) with hardly any dead cells (red), which means that the hydrogel had no cytotoxic effect. In addition, a similar density of live fibroblasts for the AgNP@GCOL/PAA group was observed in comparison to the control. Moreover, as exhibited from the optical density (OD) values in Figure 7b, the L929 fibroblasts cultured in the presence of extraction solution from AgNP@GCOL/PAA showed significant proliferation with the culture period from 1 to 3 to 5 days. Meanwhile, the OD values were close to those of the control group, confirming a good cytocompatibility of AgNP@GCOL/PAA in the cell growth environment. To further investigate the influence of AgNP@GCOL/PAA on cytoskeletal morphology, the cells cultured for 1 and 3 days were stained with fluorescein isothiocyanate (FITC)-phalloidin and 2-(4-amidinophenyl)-6-

https://doi.org/10.1021/acsami.1c21200
ACS Appl. Mater. Interfaces 2022, 14, 8728−8742

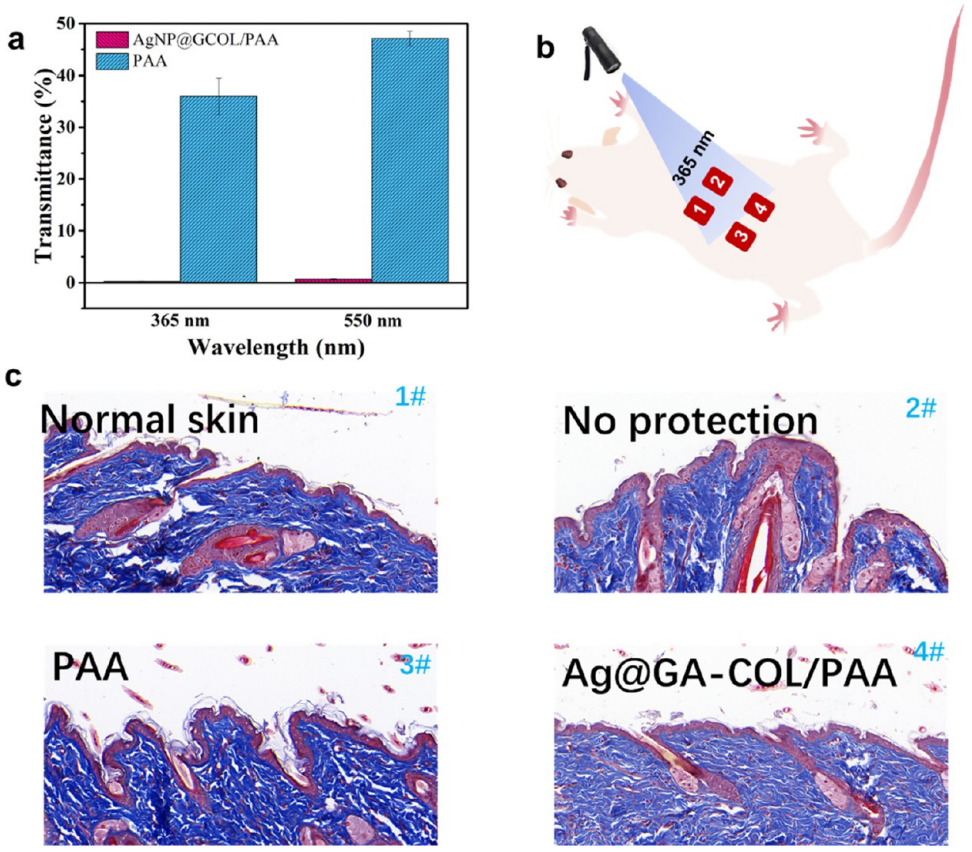

Figure 8. UV protection evaluation of AgNP@GCOL/PAA. (a) UV−Vis transmittance of PAA and AgNP@GCOL/PAA. (b) Schematic illustrating the backs of mice that suffered UV radiation at 365 nm (1#, 3#, and 4# indicate skin covered with blackout fabric, PAA, and AgNP@GCOL/PAA; 2# represents skin exposed under UV light). (c) Masson staining of dorsal mouse skin sections receiving after UV exposure.

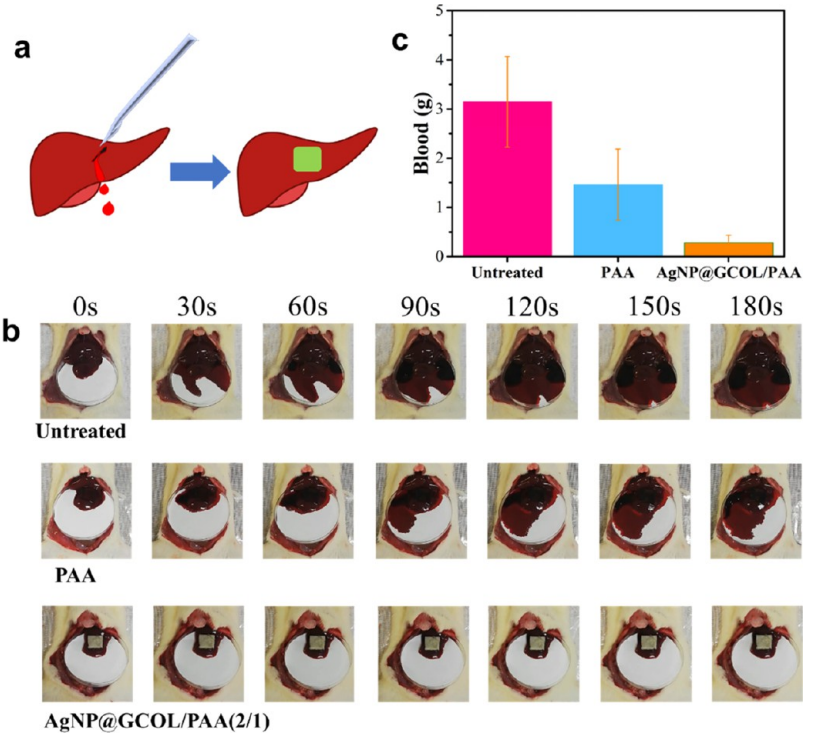

Figure 9. (a) Schematic illustrating the hemostasis effect of AgNP@GCOL/PAA(2/1). (b) Snapshots of mouse liver incision with no treatment, PAA-treatment, and AgNP@GCOL/PAA(2/1)-treatment. (c) Quantification of blood loss.

https://doi.org/10.1021/acsami.1c21200
ACS Appl. Mater. Interfaces 2022, 14, 8728−8742

indolecarbamidine dihydrochloride (DAPI) and observed using a fluorescence microscope. As shown in Figure 7c, the control sample of cells grew in a long fusiform adherent manner. The fibroblasts in the AgNP@GCOL/PAA group were polygonal, elongated, and fully stretched, which means that their cytoskeletal morphology was similar to that of the control group. Altogether, these results from in vitro cell culture showed that AgNP@GCOL/PAA is biocompatible.

Natural tissues can repair and replace tissue-engineering scaffolds throughout the whole period of regeneration, and thus the degradation rate should be matched to the repair rate of tissues to avoid too rapid or too slow dissolution.[58] The degradation profiles of AgNP@GCOL/PAA in vitro were assessed and are shown in Figure S8. At 37 °C, the hydrogels degraded gradually when incubated in the simulated body fluid as evidenced by the decreasing residual weights over time. Apparently, the ratios of GCOL/PAA had an important influence on the degradation of hydrogels. The pristine PAA showed the highest weight remaining (∼ 94% on day 12). As the fraction of GCOL increased, the weight loss increased (∼ 46% on day 12 for AgNP@GCOL/PAA(2/1)). Therefore, the degradation of GCOL contributed significantly to the weight loss of AgNP@GCOL/PAAs. The biodegradability tunable by adjusting GCOL/PAA ratios enabled AgNP@GCOL/PAA to be a more suitable adhesive for different tissues compared to the pristine PAA.[29]

AgNP@GCOL/PAA as a UV Barrier and a Hemostasis Material. Ultraviolet radiation prevention is of great significance to the healing of epidermal wound tissue. Therefore, the effect of AgNP@GCOL/PAA as a UV barrier was explored by the ultraviolet transmittance test and animal test model. Figure 8a shows that AgNP@GCOL/PAA had a higher absorption compared to PAA, which is primarily attributed to the abundance of UV-absorbing functional groups, such as phenolic groups, in AgNP@GCOL/PAA.[59] Furthermore, the large number of amide bonds in collagen allows high electron delocalization, also resulting in UV absorption.[3]

The in vivo protective effect of AgNP@GCOL/PAA against UV radiation was further investigated using an animal test model. The backs of mice were divided into four parts and simultaneously exposed to UV radiation at 365 nm for 120 min, as schematically illustrated in Figure 8b. According to the histological analysis (Figure 8c), compared with the completely occluded skin (1#), skin exposed under UV light (2#) revealed significant echinodermia and epidermal hyperplasia because of the severe UV damage. Skin covered with PAA (3#) also exhibited echinodermia and epidermal hyperplasia to some extent. In contrast, skin protected by AgNP@GCOL/PAA (4#) left the subcutaneous tissue intact. These results confirmed the excellent UV shielding properties of AgNP@GCOL/PAA. Therefore, AgNP@GCOL/PAA can effectively protect natural skin from UV damage when used as wearable devices.

To evaluate the in vivo hemostatic potential of AgNP@GCOL/PAA, we adopted a mouse hemorrhaging liver as a model (Figure 9a). For comparison, untreated and PAA-treated models were used as control groups. The difference in hemostatic performance for the three groups is revealed in Figure 9b. It could be clearly found that both the control groups showed a severe bleeding event, whereas the bleeding situation was immediately controlled after covered with AgNP@GCOL/PAA(2/1). Furthermore, the quantification of blood loss after 180 s was assessed (Figure 9c). The blood loss of AgNP@GCOL/PAA(2/1) was 0.28 ± 0.15 g, which was far lower than those of controls (3.15 ± 0.92 g for the untreated group and 1.46 ± 0.72 g for the PAA-treated group). The results indicated that AgNP@GCOL/PAA(2/1) displayed superior hemostatic properties with sharply decreasing blood loss for a mouse liver incision, closely related to its strong adhesive ability which produced the anchoring strength to the bleeding site and thus formed a network barrier with the liver tissue.[60]

CONCLUSIONS

In summary, we have reported a facile design strategy to produce a versatile collagen-based hydrogel via the introduction of a pyrogallol-Ag system. Hydrogel polymerization from AA monomers and GCOL-decorated silver nanoparticles (AgNP@GCOL) could be triggered rapidly under mild conditions though the self-catalysis effect of pyrogallol-Ag. AgNP@GCOL/PAA exhibited good toughness and stretchability. Meanwhile, the enriched reversible bonds between AgNPs, PAA, and GCOL that formed the IPN allow excellent self-healing ability, thereby significantly improving the stability of the hydrogel without structural failure. Because of the AgNPs and the polyelectrolyte (GCOL and PAA), AgNP@GCOL/PAA exhibited favorable conductivity and strain sensitivity as a flexible biosensor. In addition, because of the combined actions of AgNPs, pyrogallol, and ε-polylysine, AgNP@GCOL/PAA had an excellent antibacterial activity against both *E. coli* and *S. aureus*. Moreover, AgNP@GCOL/PAA showed good cytocompatibility and feasible UV resistance. AgNP@GCOL/PAA also displayed superior hemostatic properties, closely related to its strong adhesive ability on tissue. With the advantage of being easy to fabricate, we anticipate that the multifunctional collagen-based hydrogel provides a promising option for a broader range of applications.

MATERIALS AND METHODS

Materials. Collagen was extracted and refined from bovine split according to the method of previous work.[61] *N,N′*-Methylenebisacrylamide (MBA), silver nitrate ($AgNO_3$), ammonium hydroxide ($NH_3{\cdot}H_2O$), APS, and trypsin (≥2500 U/mg) were all purchased from Aladdin Co., Ltd. (China). Glycerol was provided by Zhiyuan Co., Ltd. (China). A live/dead cell double staining kit was purchased from Abbkine (USA). Cell Counting Kit-8 (*CCK-8*) was provided by Beyotime Biotechnology (China). Phalloidin-FTIC was purchased from Sigma-Aldrich (USA). DAPI staining solution was provided by Abcam (UK). All chemicals were of analytical grade and used as received. Deionized (DI) water was used for all aqueous samples.

Preparation of AgNP@GCOL/PAA Hydrogels. GCOL was prepared according to our previous report,[25] which was dissolved in DI water to obtain a solution of 100 mg/mL. A 20 mg/mL solution of $Ag(NH_3)_2OH$ was prepared by introducing $NH_3{\cdot}H_2O$ dropwise into $AgNO_3$ solution with a certain concentration until obtaining a limpid solution. After that, equal volumes (500 μL) of GCOL and $Ag(NH_3)_2OH$ solution were mixed to obtain AgNP@GCOL followed by the addition of AA with the volume ratio for GCOL/AA of 1:2, 1:1, and 2:1. Next, 200 μL of glycerol was introduced into the solution, and then 1 mg MBA and 35 mg APS were added and stirred. The resultant solution gelled within 15 min in a nitrogen environment. The samples were named AgNP@GCOL/PAA(1/2), AgNP@GCOL/PAA(1/1) and AgNP@GCOL/PAA(2/1) according to the volume ratio of GCOL/AA.

Characterization. The chemical structure was characterized via FTIR spectroscopy over a range of 4000−400 cm^{-1} (Nicolet IS10,

https://doi.org/10.1021/acsami.1c21200
ACS Appl. Mater. Interfaces 2022, 14, 8728−8742

Thermo Scientific, USA) with a resolution of 4 cm^{-1}. The morphology was examined using FESEM (Navo NanoSEM 230, FEI, USA), and the acceleration voltage was set to 5 kV. The crystallization information was detected with an X-ray diffractometer (D8 advance, Bruker, USA). The TEM images were collected on an emission electron microscope (TECNAIG2F20, FEI, USA). ESR spectroscopy (A300 ESR, Bruker, USA) analysis was performed by DMPO (dimethyl pyridine N oxide, free radical scavenger) trapping to characterize radicals. The electrochemical performance was obtained by CV (CHI 630E, Chenhua, Shanghai). The UV−Vis absorption of $Ag(NH_3)_2OH$ and AgNP@GCOL was examined in the range of 300−600 nm using a light transmitter (LS108H, Linshang, China) with air as the background. The swelling capacity of the dried hydrogels was studied according to a general gravimetric method. The dried hydrogels (W_d) were soaked in phosphate-buffered saline (PBS) (pH 7.4) at 37 °C. Then, the swollen hydrogels were taken out at each interval, wiped with bibulous paper carefully, and weighed (W_w). The swelling ratio was calculated by eq 1:

$$S_w\ (\%) = \frac{W_w - W_d}{W_d} \times 100\% \quad (1)$$

Mechanical Tests. Mechanical tests were conducted on a universal testing machine equipped with a 3000 N load cell (KJ-1065B, Kejian, China). Hydrogels for the tensile test were molded into dumbbell shape specimens with a gauge length, width, and thickness of 20, 10, and 2 mm, respectively, and extended at a speed of 100 mm/min. Furthermore, samples for compression testing were molded into cylindrical specimens (D = 20 mm, H = 2 mm) and used at a crosshead speed of 10 mm/min. Tensile strength and compression strength of the hydrogels were calculated based on the stress−strain curves.

The tearing test was adopted to measure the toughness of hydrogels. Rectangular hydrogel samples with 20 mm in width and 50 mm in length were cut. Afterward, an initial crack of 20 mm was cut along the midline of the hydrogel using a razor blade. The two arms of the test sample were clamped, and the one was pulled upward at a velocity 10 mm/min by grip of the tensile testing machine, while the other was maintained stationary. The tearing force F was recorded during the tearing test. The tearing energy Γ is calculated according to eq 2:[62]

$$\Gamma = \frac{2F}{t} \quad (2)$$

where F is the average tearing force (N) during steady-state tear, and t is the thickness of the specimen. Five tests were repeated for each sample to determine the toughness.

Adhesion Property Tests. Tissue adhesive strength of AgNP@GCOL/PAA was determined referring to the method from ASTM F2255-05.38. Fresh porcine skin with surface fat removed was cut into pieces of rectangular sections (12.5 × 40 mm). Next, two pieces was adhered by AgNP@GCOL/PAA with an overlapping area of 12.5 × 12.5 mm^2. This sandwich sample was pressed with a 100 g weight for 2 h at ambient temperature. After that, the adhesion strength was assessed using a universal testing machine (Kejian KJ-1065B, China) at a crosshead speed of 1 mm/min. Five parallel samples for each group were tested. The adhesion strength was calculated according to eq 3:

$$\tau = \frac{F}{s} \quad (3)$$

where τ denotes the adhesion strength (MPa), F is the tensile strength (N), and s is the overlapping area.

Electrical Tests. The simultaneous resistance changes of AgNP@GCOL/PAA were recorded with a digital electric bridge (TH2832 LCR meter, Tonghui, China). To monitor human activities, the hydrogel was attached to the fingers, shoulder, throat, and face and connected to the digital electric bridge to achieve synchronous detection. The relative resistance change was calculated according to eq 4:

$$\Delta R/R_0\ (\%) = \frac{R_s - R_0}{R_0} \times 100\% \quad (4)$$

where R_s and R_0 are the resistance when strain is applied or not, respectively.

Antibacterial Activity Tests. The surface antibacterial activity of AgNP@GCOL/PAA against *S. aureus* and *E. coli* was determined based on the reference with slight modification.[63] In brief, 10 mL of bacteria suspension in sterilized PBS (10^6 CFU/mL) was dispersed onto a tryptic soy/LB agar plate (Φ70 × 7 mm). Each AgNP@GCOL/PAA disk (Φ 5 × 3 mm) was mounted in the center of an agar plate and incubated at 37 °C. After 24 h incubation, the diameter of the bacteriostatic rings around disks was recorded, and the colony-forming units on the agar plate were counted to calculate the bacterial kill ratio.

In Vitro Cell Culture. The cytocompatibility of the hydrogels was evaluated by live/dead viability, cytotoxicity assay, and cytoskeletal staining. First, 200 mg of the hydrogel was incubated in 2 mL of PBS for 24 h at 37 °C. Then, the leach solution on the top was collected and used as the hydrogel extract. Mouse fibroblast cells (L929) were seeded in a 96-well plate (1×10^4 per well) and incubated in Dulbecco's modified Eagle's medium containing 10% fetal bovine serum under the standard culture conditions of 37 °C and 5% CO_2 for 24 h. Then, the cell medium was removed, and a fresh medium containing hydrogel extract was added into the 96-well plate. Controls were prepared by incubating cell-laden hydrogels in culture medium with 0.5% Triton X-100. Cells were cultured for another 48 h, and afterward, 300 μL of live/dead reagent was then added into each well, and finally the cell morphology was observed and imaged using a fluorescence microscope (Nikon, Ti-E, Japan).

The CCK-8 method was used to estimate the cell viability. First, 8000 cells (L929) were cultured in each well of 96-well plates at 37 °C with 5% CO_2 for 24 h. Then the cells were cultured with or without hydrogel extract in the complete growth medium for 1, 3, and 5 days. At each time point, the spent medium was discarded followed by addition of a fresh medium that contained 10% CCK-8 solution into each well. After 3 h of reaction in a 5% CO_2 incubator at 37 °C, 100 μL supernatant was transferred into a 96-well plate to be measured at 450 nm using a microplate reader (BioTek, EL × 800, USA).

To further observe the cytoskeletal morphology of cells, cells cultured in the complete growth medium containing hydrogel extract for 1 and 3 days were stained by FITC-labeled phalloidin and DAPI for F-Actin and nuclei, respectively. Samples were washed with PBS, fixed with 4% formalin, and permeabilized with 0.2% Triton X-100 in PBS. Then, the cells were stained with phalloidin-FITC to reveal actin organization and DAPI to show the nuclei. The images were collected using a confocal microscope (ZEISS, LSM700, Germany) with the fluorescence signal from phalloidin-FITC and DAPI.

In Vitro Degradation. In vitro degradation tests were carried out by an enzymatic assay under simulated physiological conditions. Briefly, 100 mg of samples (W_0) was immersed in 10 mL of simulated body fluid (pH 7.4) containing 10 mg of trypsin and then shaken at 60 rpm, 37 °C in a shaker. At each predetermined time interval, the samples were collected by centrifugation, washed several times with DI water, and finally lyophilized and weighed (W_t). At each time interval, the percentage of weight remaining was calculated by eq 5:

$$W_r\ (\%) = \frac{W_t}{W_0} \times 100\% \quad (5)$$

UV Protection Tests. For in vivo UV barrier properties, BALB/c mice (25−30 g) were chosen as the experimental model. The operational steps are outlined below: the mice were anesthetized and fixed on an operating table, whose back was shaved and compartmentalized into four sections of 1 × 1 cm^2. Then the mice were administered with the same mass of PAA (H = 2 mm), AgNP@GCOL/PAA(2/1) (H = 2 mm), masking with a bezel, or exposing thoroughly. Subsequently, the marked areas of the skin were then exposed to 30 mW/cm^2 of UV (365 nm) irradiation for 120 min. The distance between the mouse dorsal skin and the lamp was 10 cm.

https://doi.org/10.1021/acsami.1c21200
ACS Appl. Mater. Interfaces 2022, 14, 8728−8742

After that, the irradiated skin was harvested after the mice were euthanized followed by tissue section processing according to a previous study.[25] Masson staining was applied before observation with an inverted microscope (Nikon Eclipse E100, Japan).

Hemostatic Ability Tests. The hemostatic effect of AgNP@GCOL/PAA was evaluated in a mouse liver hemorrhaging model according to the previous report.[64] Briefly, the enterocoelia of Sprague Dawley mice (180~220 g) were opened, leading to exposure of the liver. After that, a liver incision of 8 and 2 mm in length and width respectively was created with a surgical knife. After 10 s, AgNP@GCOL/PAA was covered at the bleeding site and the blood loss was recorded within 180 s. The untreated and PAA-treated groups were used as controls.

These tests were performed strictly in compliance with the guidelines of Animal Experiment Ethics Committee of Fujian Agriculture and Forestry University.

■ ASSOCIATED CONTENT

Supporting Information

The Supporting Information is available free of charge at https://pubs.acs.org/doi/10.1021/acsami.1c21200.

The characteristic peaks from FTIR spectra of samples; the conductivity of AgNP@GCOL/PAA; swelling behaviors of AgNP@GCOL/PAA; digital photos illustrating the excellent self-recovery ability of AgNP@GCOL/PAA; tear curve and tearing energy of AgNP@GCOL/PAA; G′ and G″ of AgNP@GCOL/PAA from dynamic oscillation sweep; the residual weight of AgNP@GCOL/PAA with increasing storage times; digital photos showing that the self-adhesive AgNP@GCOL/PAA was residue-free and nonallergic; response to pen tip pressure of AgNP@GCOL/PAA as an on-skin sensor; and in vitro degradation behavior of AgNP@GCOL/PAA (PDF)

■ AUTHOR INFORMATION

Corresponding Authors

Lihui Chen − *College of Materials Engineering, Fujian Agriculture and Forestry University, Fuzhou 350002, PR China*; Phone: +86 0591 83715175; Email: fafuclh@163.com

Hui Wu − *College of Materials Engineering, Fujian Agriculture and Forestry University, Fuzhou 350002, PR China*; orcid.org/0000-0002-9755-8371; Phone: +86 0591 83715175; Email: wuhuifafu@163.com

Cuicui Ding − *College of Ecological Environment and Urban Construction, Fujian University of Technology, Fuzhou 350108, PR China*; orcid.org/0000-0002-4785-6629; Phone: +86 0591 22863260; Email: dingcuicui.1124@163.com

Authors

Min Zhang − *College of Materials Engineering, Fujian Agriculture and Forestry University, Fuzhou 350002, PR China; National Forestry & Grassland Administration Key Laboratory for Plant Fiber Functional Materials, Fuzhou 350002, PR China*; orcid.org/0000-0001-7117-8007

Qili Yang − *College of Materials Engineering, Fujian Agriculture and Forestry University, Fuzhou 350002, PR China*

Tianshuo Hu − *College of Materials Engineering, Fujian Agriculture and Forestry University, Fuzhou 350002, PR China*

Lele Tang − *College of Materials Engineering, Fujian Agriculture and Forestry University, Fuzhou 350002, PR China*

Yonghao Ni − *College of Materials Engineering, Fujian Agriculture and Forestry University, Fuzhou 350002, PR China; Department of Chemical Engineering and Limerick Pulp & Paper Centre, University of New Brunswick, Fredericton E3B 5A3, Canada*; orcid.org/0000-0001-6107-6672

Liulian Huang − *College of Materials Engineering, Fujian Agriculture and Forestry University, Fuzhou 350002, PR China*; orcid.org/0000-0003-3158-593X

Complete contact information is available at: https://pubs.acs.org/10.1021/acsami.1c21200

Author Contributions

The manuscript was written through contributions of all authors. All authors have given approval to the final version of the manuscript.

Notes

The authors declare no competing financial interest.

■ ACKNOWLEDGMENTS

This work was financially supported by the National Natural Science Foundation of China (Grant No. 22178056 and 22078060), the Natural Science Foundation of Fujian Province (Grant No. 2020 J01555 and 2020 J01881), the Opening Project of Guangxi Key Laboratory of Clean Pulp & Papermaking and Pollution Control (2019KF09), and Special Fund for Science and Technology Innovation of Fujian Agriculture and Forestry University (Grant Nos. CXZX2019108S and CXZX2019116G).

■ REFERENCES

(1) Chen, C.; Changyou, S.; Lei, M.; Jun, Y. High-Strength, Self-Adhesive, and Strain-Sensitive Chitosan/Poly(acrylic acid) Double-Network Nanocomposite Hydrogels Fabricated by Salt-Soaking Strategy for Flexible Sensors. *ACS Appl. Mater. Interfaces* **2019**, *11*, 39228−39237.

(2) Chen, S.; Zeng, S.; Liu, S.; Liu, H.; Zheng, R.; White, K. L.; Smith, A. T.; Liu, L.; Sun, L. A Biomimetic Interface with High Adhesion, Tailorable Modulus for On-Skin Sensors, and Low-Power Actuators. *Chem. Mater.* **2019**, *31*, 8708−8716.

(3) Wang, R.; Wang, X.; Zhan, Y.; Xu, Z.; Xu, Z.; Feng, X.; Li, S.; Xu, H. A Dual Network Hydrogel Sunscreen Based on Poly-γ-glutamic Acid/Tannic Acid Demonstrates Excellent Anti-UV, Self-Recovery, and Skin-Integration Capacities. *ACS Appl. Mater. Interfaces* **2019**, *11*, 37502−37512.

(4) Liao, H.; Guo, X.; Wan, P.; Yu, G. Conductive MXene Nanocomposite Organohydrogel for Flexible, Healable, Low-Temperature Tolerant Strain Sensors. *Adv. Funct. Mater.* **2019**, *29*, No. 1904507.

(5) Wang, Y.; Zhang, L.; Lu, A. Transparent, Antifreezing, Ionic Conductive Cellulose Hydrogel with Stable Sensitivity at Subzero Temperature. *ACS Appl. Mater. Interfaces* **2019**, *11*, 41710−41716.

(6) Yuk, H.; Zhang, T.; Parada, G. A.; Liu, X.; Zhao, X. Skin-inspired Hydrogel−elastomer Hybrids with Robust Interfaces and Functional Microstructures. *Nat. Commun.* **2016**, *7*, 12028.

(7) Yuk, H.; Varela, C. E.; Nabzdyk, C. S.; Mao, X.; Padera, R. F.; Roche, E. T.; Zhao, X. Dry Double-sided Tape for Adhesion of Wet tissues and Devices. *Nature* **2019**, *575*, 169−174.

(8) Desai, M. S.; Chen, M.; Hong, F. H. J.; Lee, J. H.; Wu, Y.; Lee, S.-W. Catechol-functionalized Elastin-like Polypeptides as Tissue Adhesives. *Biomacromolecules* **2020**, *21*, 2938−2948.

(9) Tian, M. P.; Zhang, A. D.; Yao, Y. X.; Chen, X. G.; Liu, Y. Mussel-inspired Adhesive and Polypeptide-based Antibacterial Thermo-sensitive Hydroxybutyl Chitosan Hydrogel as BMSCs 3D Culture Matrix for Wound Healing. *Carbohydr. Polym.* **2021**, *261*, No. 117878.
(10) Wei, K.; Senturk, B.; Matter, M. T.; Wu, X.; Herrmann, I. K.; Rottmar, M.; Toncelli, C. Mussel-Inspired Injectable Hydrogel Adhesive Formed under Mild Conditions Features Near-Native Tissue Properties. *ACS Appl. Mater. Interfaces* **2019**, *11*, 47707−47719.
(11) Lu, X.; Shi, S.; Li, H.; Gerhard, E.; Lu, Z.; Tan, X.; Li, W.; Rahn, K. M.; Xie, D.; Xu, G.; Zou, F.; Bai, X.; Guo, J.; Yang, J. Magnesium Oxide-crosslinked Low-swelling Citrate-based Mussel-inspired Tissue Adhesives. *Biomaterials* **2020**, *232*, No. 119719.
(12) Filippidi, E.; Cristiani, T. R.; Eisenbach, C. D.; Waite, J. H.; Israelachvili, J. N.; Ahn, B. K.; Valentine, M. T. Toughening Elastomers using Mussel-inspired Iron-catechol Complexes. *Science* **2017**, *358*, 502.
(13) Deng, X.; Huang, B.; Wang, Q.; Wu, W.; Coates, P.; Sefat, F.; Lu, C.; Zhang, W.; Zhang, X. A Mussel-Inspired Antibacterial Hydrogel with High Cell Affinity, Toughness, Self-Healing, and Recycling Properties for Wound Healing. *ACS Sustainable Chem. Eng.* **2021**, *9*, 3070−3082.
(14) Fang, G.; Gao, J.; Dionysiou, D. D.; Liu, C.; Zhou, D. Activation of Persulfate by Quinones: Free Radical Reactions and Implication for the Degradation of PCBs. *Environ. Sci. Technol.* **2013**, *47*, 4605−4611.
(15) Lovley, D. R.; Blunthariss, E. L.; Ejp, P.; Woodward, J. C.; Coates, J. D. Humic Substances as Electron Acceptors for Microbial Respiration. *Nature* **1996**, *382*, 445−448.
(16) Guo, J.; Sun, W.; Kim, J. P.; Lu, X.; Li, Q.; Lin, M.; Mrowczynski, O.; Rizk, E. B.; Cheng, J.; Qian, G. Development of Tannin-inspired Antimicrobial Bioadhesives. *Acta Biomater.* **2018**, 35−44.
(17) Bicchieri, M.; Monti, M.; Piantanida, G.; Sodo, A. Non-destructive Spectroscopic Investigation on Historic Yemenite Scriptorial Fragments: Evidence of Different Degradation and Recipes for Iron Tannic Inks. *Anal. Bioanal. Chem.* **2013**, *405*, 2713−2721.
(18) Lee, A. S.; Mahon, P. J.; Creagh, D. C. Raman Analysis of Iron Gall Inks on Parchment. *Vib. Spectrosc.* **2006**, *41*, 170−175.
(19) Kumari, H.; Kline, S. R.; Dennis, C. L.; Mossine, A. V.; Paul, R. L.; Deakyne, C. A.; Atwood, J. L. Titelbild: Solution-phase and Magnetic Approach towards Understanding Iron Gall Ink-like Nanoassemblies. *Am. Ethnol.* **2012**, *51*, 9263−9266.
(20) Kustin, K.; Nicolini, C.; Toppen, D. L. Interaction of Catechol and Catechol Derivatives with Dioxovanadium(V). II. Kinetics of Ligand Oxidation. *J. Am. Chem. Soc.* **1974**, *96*, 7416−7420.
(21) Hino, Y.; Ejima, H. Tissue Adhesive Properties of Functionalized Chitosan: A Comparative Study of Phenol, Catechol and Gallol. *J. Photopolym. Sci. Technol.* **2020**, *33*, 123−127.
(22) Oh, X. D.; Kim, S.; Lee, D.; Hwang, D. S. Tunicate-mimetic Nanofibrous Hydrogel Adhesive with Improved Wet Adhesion. *Acta Biomater.* **2015**, *20*, 104−112.
(23) Sautrot-Ba, P.; Malval, J. P.; Weiss-Maurin, M.; Paul, J.; Blacha-Grzechnik, A.; Tomane, S.; Mazeran, P. E.; Lalevée, J.; Langlois, V.; Versace, D. L. Paprika, Gallic Acid and Visible Light: the Green Combination for the Synthesis of Biocide Coatings. *ACS Sustainable Chem. Eng.* **2018**, *6*, 104−109.
(24) Sorushanova, A.; Delgado, L. M.; Wu, Z.; Shologu, N.; Kshirsagar, A.; Raghunath, R.; Mullen, A. M.; Bayon, Y.; Pandit, A.; Raghunath, M.; Zeugolis, D. I. The Collagen Suprafamily: From Biosynthesis to Advanced Biomaterial Development. *Adv. Mater.* **2019**, *31*, No. 1801651.
(25) Yang, Q.; Tang, L.; Guo, C.; Deng, F.; Wu, H.; Chen, L.; Huang, L.; Lu, P.; Ding, C.; Ni, Y.; Zhang, M. A Bioinspired Gallol-functionalized Collagen as Wet-tissue Adhesive for Biomedical Applications. *Chem. Eng. J.* **2021**, *417*, No. 127962.
(26) Liu, Y. J.; Cao, W. T.; Ma, M. G.; Wan, P. Ultrasensitive Wearable Soft Strain Sensors of Conductive, Self-healing, and Elastic Hydrogels with Synergistic "Soft and Hard" Hybrid Networks. *ACS Appl. Mater. Interfaces* **2017**, *9*, 25559−25570.
(27) Jing, X.; Mi, H.-Y.; Lin, Y.-J.; Enriquez, E.; Peng, X.-F.; Turng, L.-S. Highly Stretchable and Biocompatible Strain Sensors Based on Mussel-Inspired Super-Adhesive Self-Healing Hydrogels for Human Motion Monitoring. *ACS Appl. Mater. Interfaces* **2018**, *10*, 20897.
(28) Ma, S.; Yan, C.; Cai, M.; Yang, J.; Wang, X.; Zhou, F.; Liu, W. Continuous Surface Polymerization via Fe(II)-Mediated Redox Reaction for Thick Hydrogel Coatings on Versatile Substrates. *Adv. Mater.* **2018**, *30*, No. e1803371.
(29) Li, J.; Yu, F.; Chen, G.; Liu, J.; Li, X.-L.; Cheng, B.; Mo, X.-M.; Chen, C.; Pan, J.-F. Moist-Retaining, Self-Recoverable, Bioadhesive, and Transparent in Situ Forming Hydrogels To Accelerate Wound Healing. *ACS Appl. Mater. Interfaces* **2020**, *12*, 2023−2038.
(30) Chen, K.; Lin, Q.; Wang, L.; Zhuang, Z.; Zhang, Y.; Huang, D.; Wang, H. An All-in-One Tannic Acid-Containing Hydrogel Adhesive with High Toughness, Notch Insensitivity, Self-Healability, Tailorable Topography, and Strong, Instant, and On-demand Underwater Adhesion. *ACS Appl. Mater. Interfaces* **2021**, *13*, 9748−9761.
(31) Xu, Q.; Jin, L.; Wang, Y.; Hao, C.; Qin, M. Synthesis of Silver Nanoparticles using Dialdehyde Cellulose Nanocrystal as a Multi-functional Agent and Application to Antibacterial Paper. *Cellulose* **2019**, *26*, 1309−1321.
(32) Gan, D.; Xing, W.; Jiang, L.; Fang, J.; Zhao, C.; Ren, F.; Fang, L.; Wang, K.; Lu, X. Plant-inspired Adhesive and Tough Hydrogel Based on Ag-Lignin Nanoparticles-triggered Dynamic Redox Catechol Chemistry. *Nat. Commun.* **2019**, *10*, 1487.
(33) Feig, V. R.; Tran, H.; Lee, M.; Bao, Z. Mechanically Tunable Conductive Interpenetrating Network Hydrogels that Mimic the Elastic Moduli of Biological Tissue. *Nat. Commun.* **2018**, *9*, 2740.
(34) Hu, X.; Xia, X.-X.; Huang, S.-C.; Qian, Z.-G. Development of Adhesive and Conductive Resilin-Based Hydrogels for Wearable Sensors. *Biomacromolecules* **2019**, *20*, 3283−3293.
(35) Jiang, P.; Lin, P.; Yang, C.; Qin, H.; Wang, X.; Zhou, F. 3D Printing of Dual-Physical Cross-linking Hydrogel with Ultrahigh Strength and Toughness. *Chem. Mater.* **2020**, *32*, 9983−9995.
(36) Ni, X.; Yang, Z.; Li, J. Scaling Behavior of Fracture Properties of Tough Adhesive Hydrogels. *ACS Macro Lett.* **2021**, *10*, 180−185.
(37) Chen, K.; Feng, Y.; Zhang, Y.; Yu, L.; Hao, X.; Shao, F.; Dou, Z.; An, C.; Zhuang, Z.; Luo, Y.; Wang, Y.; Wu, J.; Ji, P.; Chen, T.; Wang, H. Entanglement-Driven Adhesion, Self-Healing, and High Stretchability of Double-Network PEG-Based Hydrogels. *ACS Appl. Mater. Interfaces* **2019**, *11*, 36458−36468.
(38) Xin, Z.; Zhang, M.; Guo, B.; Ma, P. X. Mussel-inspired Injectable Supramolecular and Covalent Bonds Crosslinked Hydrogels with Rapid Self-healing and Recovery via a Facile Approach Under Metal-free Conditions. *J. Mater. Chem. B* **2016**, *4*, 6644−6651.
(39) Zhang, M.; Deng, F.; Tang, L.; Wu, H.; Ni, Y.; Chen, L.; Huang, L.; Hu, X.; Lin, S.; Ding, C. Super-ductile, Injectable, Fast Self-healing Collagen-based Hydrogels with Multi-responsive and Accelerated Wound-repair Properties. *Chem. Eng. J.* **2021**, *405*, No. 126756.
(40) Güner, S.; Gürbüz, O.; Çalışkan, S.; Nuzhdin, V. I.; Khaibullin, R.; Öztürk, M.; Akdoğan, N. The Structural and Magnetic Properties of Co^{+} Implanted ZnO Films. *Appl. Surf. Sci.* **2014**, *310*, 235−241.
(41) Xu, J.; Jin, R.; Duan, L.; Ren, X.; Gao, G. Tough, Adhesive and Conductive Polysaccharide Hydrogels Mediated by Ferric Solution. *Carbohydr. Polym.* **2019**, *211*, 1−10.
(42) Chen, H.; Ren, X.; Gao, G. Skin-inspired Gels with Toughness, Antifreezing, Conductivity, and Remoldability. *ACS Appl. Mater. Interfaces* **2019**, *11*, 28336−28344.
(43) Ding, X.; Li, G.; Zhang, P.; Jin, E.; Xiao, C.; Chen, X. Injectable Self-Healing Hydrogel Wound Dressing with Cysteine-Specific On-Demand Dissolution Property Based on Tandem Dynamic Covalent Bonds. *Adv. Funct. Mater.* **2021**, *31*, No. 2011230.
(44) Li, S.; Wang, L.; Zheng, W.; Yang, G.; Jiang, X. Rapid Fabrication of Self-healing, Conductive, and Injectable Gel as Dressings for Healing Wounds in Stretchable Parts of the Body. *Adv. Funct. Mater.* **2020**, *30*, No. 2002370.

https://doi.org/10.1021/acsami.1c21200
ACS Appl. Mater. Interfaces 2022, 14, 8728−8742

(45) Zhang, B.; He, J.; Shi, M.; Liang, Y.; Guo, B. Injectable Self-healing Supramolecular Hydrogels with Conductivity and Photothermal Antibacterial Activity to Enhance Complete Skin Regeneration. *Chem. Eng. J.* **2020**, *400*, No. 125994.
(46) Figueiredo, T.; Jing, J.; Jeacomine, I.; Olsson, J.; Gerfaud, T.; Boiteau, J.-G.; Rome, C.; Harris, C.; Auzély-Velty, R. Injectable Self-healing Hydrogels Based on Boronate Ester Formation between Hyaluronic Acid Partners Modified with Benzoxaborin Derivatives and Saccharides. *Biomacromolecules* **2020**, *21*, 230−239.
(47) Han, L.; Liu, K.; Wang, M.; Wang, K.; Fang, L.; Chen, H.; Zhou, J.; Lu, X. Mussel-Inspired Adhesive and Conductive Hydrogel with Long-Lasting Moisture and Extreme Temperature Tolerance. *Adv. Funct. Mater.* **2018**, *28*, No. 1704195.
(48) Yang, J.; Bai, R.; Chen, B.; Suo, Z. Hydrogel Adhesion: A Supramolecular Synergy of Chemistry, Topology, and Mechanics. *Adv. Funct. Mater.* **2020**, *30*, No. 1901693.
(49) Deng, J.; Tang, Y.; Zhang, Q.; Wang, C.; Liao, M.; Ji, P.; Song, J.; Luo, G.; Chen, L.; Ran, X.; Wei, Z.; Zheng, L.; Dang, R.; Liu, X.; Zhang, H.; Zhang, Y. S.; Zhang, X.; Tan, H. A Bioinspired Medical Adhesive Derived from Skin Secretion of Andrias davidianus for Wound Healing. *Adv. Funct. Mater.* **2019**, *29*, No. 1809110.
(50) Zhao, Q.; Mu, S.; Long, Y.; Zhou, J.; Gu, H. Tannin-Tethered Gelatin Hydrogels with Considerable Self-Healing and Adhesive Performances. *Macromol. Mater. Eng.* **2019**, *304*, No. 1800664.
(51) Zhan, K.; Kim, C.; Sung, K.; Ejima, H.; Yoshie, N. Tunicate-Inspired Gallol Polymers for Underwater Adhesive: A Comparative Study of Catechol and Gallol. *Biomacromolecules* **2017**, *18*, 2959−2966.
(52) Lu, Q.; Soo Hwang, D.; Liu, Y.; Zeng, H. Molecular Interactions of Mussel Protective Coating Protein, Mcfp-1, from Mytilus californianus. *Biomaterials* **2012**, *33*, 1903−1911.
(53) Liu, S.; Zheng, R.; Chen, S.; Wu, Y.; Liu, H.; Wang, P.; Deng, Z.; Liu, L. A Compliant, Self-adhesive and Self-healing Wearable Hydrogel as Epidermal Strain Sensor. *J. Mater. Chem. C* **2018**, *6*, 4183−4190.
(54) Haidari, H.; Bright, R.; Strudwick, X. L.; Garg, S.; Kopecki, Z. Multifunctional Ultrasmall AgNP Hydrogel Accelerates Healing of S. aureus Infected Wounds. *Acta Biomater.* **2021**, *128*, 420−434.
(55) Sun, X.; Dong, M.; Guo, Z.; Zhang, H.; Wang, J.; Jia, P.; Bu, T.; Liu, Y.; Li, L.; Wang, L. Multifunctional Chitosan-copper-gallic acid based Antibacterial Nanocomposite Wound Dressing. *Int. J. Biol. Macromol.* **2021**, *167*, 10−22.
(56) Bhattacharya, S.; Dineshkumar, R.; Dhanarajan, G.; Sen, R.; Mishra, S. Improvement of ε-polylysine Production by Marine Bacterium Bacillus licheniformis using Artificial Neural Network Modeling and Particle Swarm Optimization Technique. *Biochem. Eng. J.* **2017**, *126*, 8−15.
(57) Xing, R.; Li, S.; Zhang, N.; Shen, G.; Möhwald, H.; Yan, X. Self-Assembled Injectable Peptide Hydrogels Capable of Triggering Antitumor Immune Response. *Biomacromolecules* **2017**, *18*, 3514−3523.
(58) Liu, X.; He, X.; Jin, D.; Wu, S.; Wang, H.; Yin, M.; Aldalbahi, A.; El-Newehy, M.; Mo, X.; Wu, J. A Biodegradable Multifunctional Nanofibrous Membrane for Periodontal Tissue Regeneration. *Acta Biomater.* **2020**, *108*, 207−222.
(59) Castagna, A.; Csepregi, K.; Neugart, S.; Zipoli, G.; Večeřová, K.; Jakab, G.; Jug, T.; Llorens, L.; Martínez-Abaigar, J.; Martínez-Lüscher, J.; Núñez-Olivera, E.; Ranieri, A.; Schoedl-Hummel, K.; Schreiner, M.; Teszlák, P.; Tittmann, S.; Urban, O.; Verdaguer, D.; Jansen, M. A. K.; Hideg, É. Environmental Plasticity of Pinot Noir Grapevine Leaves: A Trans-European Study of Morphological and Biochemical Changes along a 1,500-km Latitudinal Climatic Gradient. *Plant, Cell Environ.* **2017**, *40*, 2790−2805.
(60) Gu, B. K.; Park, S. J.; Kim, M. S.; Lee, Y. J.; Kim, J.-I.; Kim, C.-H. Gelatin Blending and Sonication of Chitosan Nanofiber Mats Produce Synergistic Effects on Hemostatic Functions. *Int. J. Biol. Macromol.* **2016**, *82*, 89−96.
(61) Zhang, M.; Yang, J.; Yang, Q.; Huang, L.; Wu, H.; Chen, L.; Ding, C. Fluorescence Studies on the Aggregation Behaviors of Collagen Modified with NHS-activated Poly(γ-glutamic acid). *Int. J. Biol. Macromol.* **2018**, *112*, 1156−1163.
(62) Liang, S.; Hu, J.; Wu, Z. L.; Kurokawa, T.; Gong, J. P. Toughness Enhancement and Stick−Slip Tearing of Double-Network Hydrogels in Poly(ethylene glycol) Solution. *Macromolecules* **2012**, *45*, 4758−4763.
(63) Li, G.; Yu, S.; Xue, W.; Ma, D.; Zhang, W. Chitosan-graft-PAMAM Loading Nitric Oxide for Efficient Antibacterial Application. *Chem. Eng. J.* **2018**, *347*, 923−931.
(64) Ding, C.; Tian, M.; Feng, R.; Dang, Y.; Zhang, M. Novel Self-Healing Hydrogel with Injectable, pH-Responsive, Strain-Sensitive, Promoting Wound-Healing, and Hemostatic Properties Based on Collagen and Chitosan. *ACS Biomater. Sci. Eng.* **2020**, *6*, 3855−3867.

https://doi.org/10.1021/acsami.1c21200
ACS Appl. Mater. Interfaces 2022, 14, 8728−8742